Monthly Notices
of the
ROYAL ASTRONOMICAL SOCIETY

Mon. Not. R. Astron. Soc. (2010) doi:10.1111/j.1365-2966.2010.16805.x

Final verdict from *XMM–Newton*: the X-ray obscured Seyfert galaxy NGC 5506 has a broad Fe K_α line

M. Guainazzi,[1⋆] S. Bianchi,[2] G. Matt,[2] M. Dadina,[3] J. Kaastra,[4] J. Malzac[5] and G. Risaliti[6,7]

[1] *European Space Astronomy Centre of the Europaen Space Agency, PO Box 78, Villanueva de la Cañada, E-28691 Madrid, Spain*
[2] *Dipartimento di Fisica, Universitá degli Studi Roma Tre, via della Vasca Navale 84, I-00046 Roma, Italy*
[3] *INAF/IASF-Bo, via Gobetti 101, I-40129 Bologna, Italy*
[4] *SRON Netherlands Institute for Space Research, Sorbonnelaan 2, 3584 CA Utrecht, the Netherlands*
[5] *Centre d'Etude Spatiale des Rayonnements, Université de Toulouse, CNRS, 9 Avenue du Colonel Roche, BP 44346, 31028 Toulouse Cedex 4, France*
[6] *Harvard-Smithsonian Center for Astrophysics, 60 Garden St, Cambridge, MA 02138, USA*
[7] *INAF-Osservatorio di Arcetri, Largo E. Fermi 5, I-50125, Firenze, Italy*

Accepted 2010 April 7. Received 2010 April 7; in original form 2009 November 23

ABSTRACT

We present the first unambiguous evidence of a broad (Gaussian width ∼330 eV) component of the iron K_α fluorescent emission line in the X-ray obscured narrow-line Seyfert 1 galaxy, NGC 5506. This is the main result of a spectroscopic monitoring campaign on this source, performed with the *XMM–Newton* observatory between 2001 February and 2009 January. The broad line lacks extreme redward skewness. If modelled with a relativistic component, the profile of the line is consistent with a flat emissivity radial dependence ($\alpha \simeq 1.9$). The disc inclination ($\simeq 40^\circ$) is nominally larger than typically observed in unobscured active galactic nuclei (AGNs), in agreement with most measurements of broadened iron lines in Seyfert 2 galaxies. The quality of the data allows us to decompose the full iron emission-line complex, and to study its long-term (time-scales of weeks to yr) variability pattern. The intensity of the neutral and narrow iron K_α core remains constant during the monitoring campaign. This indicates that the optically thick gas responsible for the non-relativistic reprocessing of the primary AGN continuum in NGC 5506 is probably located in the torus rather than in the optical broad-line region.

Key words: galaxies: active – galaxies: Seyfert – X-rays: galaxies – X-rays: individual: NGC 5506.

1 INTRODUCTION

The broadening by relativistic effects of emission lines in an X-ray illuminated accretion disc offers us the opportunity to probe the physical conditions and geometrical distribution of matter in the vicinity of black holes, as well as general relativity effects (Reynolds & Nowak 2003; Miller 2007). Broad and skewed profiles of the iron K_α fluorescent emission line were discovered by *ASCA* in the mid-1990s (Mushotzky et al. 1995; Tanaka et al. 1995). High-throughput observations with the EPIC cameras on board *XMM–Newton* have shown that at least 30 per cent of nearby Seyfert galaxies exhibit relativistically blurred features, consistent with being produced within 50 gravitational radii ($r_g \equiv GM/c^2$, where M is the black hole mass; Nandra et al. 2007). However, doubts have been cast on the robustness and uniqueness of these results. Ionized outflows partially covering the primary high-energy emission in active galactic nuclei (AGNs) could mimic relativistic effects (Reeves et al. 2004; Turner & Miller 2009). Controversy is fierce. In this context, it is crucial to confirm whether objects, whose data have poor signal-to-noise, do exhibit relativistically broadened lines and also to expand the parameter space covered by these measurements.

The study of X-ray obscured AGNs is particularly promising. In the 'unified model' framework (Antonucci & Miller 1985; Antonucci 1993), their putative accretion discs are expected to be observed at higher inclination angles if the plane of the disc is aligned with that of the obscuring matter. For inclinations not too close to 'edge-on', special relativistic effects, such as Doppler boosting, should therefore be stronger and easier to detect. Moreover, in type II objects, the polar outflows should be out of the line of sight, and this should break the degeneracy between 'warm absorbers' and relativistic lines (Turner & Miller 2009). Finally, relativistic lines allow direct measurements of the inclination angle of the accretion disc, thus offering a simple test of the unified scenarios.

⋆E-mail: Matteo.Guainazzi@sciops.esa.int

Table 1. Log of *XMM–Newton* NGC 5506 observations.

XMM–Newton ID	Start time	ρ^a (arcsec)	$T^b_{\rm CR}$ (s^{-1})	$T^c_{\rm exp}$ (ks)
0013140101 (1)[d]	2001-02-02	100/40	0.2/0.5	13.3
0013140201 (2)[d]	2002-01-09	120/44	0.5/1.0	9.9
0201830201 (3)[d]	2004-07-11	42/45	0.5/0.5	14.8
0201830301 (4)[d]	2004-07-14	40/42	0.5/0.35	13.9
0201830401 (5)[d]	2004-07-22	40/42	0.35/0.35	13.8
0201830501 (6)[d]	2004-08-07	40/42	0.35/0.35	13.9
0554170101 (7)[d]	2008-07-27	50/50	0.35/0.35	55.8
0554170201 (8)[d]	2009-01-02	40/40	0.5/0.35	62.0

[a]Size of the source spectrum extraction region in the MOS/pn.
[b]Count rate threshold applied to select intervals of low particle background in the MOS/pn.
[c]The pn exposure time.
[d]The label used to identify the observation in this paper: XMM*i*.

Observations of the broad Fe line in X-ray obscured Seyferts have so far been sparse. The Fe K_α line in the *Suzaku* spectrum of MCG-5-23-16 implies a disc inclination, $\imath$, of $53^\circ \pm ^{7}_{9}{}^\circ$ (Reeves et al. 2007).[1] Nandra et al. (2007) add to this census NGC 526A ($\imath = 43^\circ \pm ^{42}_{20}{}^\circ$) and NGC 2992 ($\imath = 24^\circ \pm 7^\circ$), whereas NGC 2110 and Mkn 6 do not exhibit significant evidence for relativistic effects. NGC 1365 ($\imath = 24^\circ \pm ^{8}_{4}{}^\circ$; Risaliti et al. 2009) and IRAS 13197–1627 ($\imath = 27^\circ \pm 17^\circ$; Dadina & Cappi 2004; Miniutti et al. 2007b) were also recently discovered to host broad lines from nominally low inclination discs. The aforementioned uncertainties are purely statistics; systematic uncertainties related, for example, to different spectral deconvolutions are seldom discussed in the literature. These can be at least comparable to the statistical uncertainties.

In this context, the case of the nearby ($z = 0.0061$) X-ray obscured ($N_{\rm H} \simeq 3 \times 10^{22}$ cm^{-2}; Wang et al. 1999) narrow-line Seyfert 1 galaxy (NLSy1; Nagar et al. 2002) NGC 5506 is one of the most controversial. Bianchi et al. (2003) analysed all the X-ray observations of NGC 5506 performed with imaging and spectroscopic instruments at that time. They did not detect any spectral components directly related to the accretion disc. This led them to conclude that the disc is either fully ionized, or almost edge-on. Two early *XMM–Newton* observations of NGC 5506 (originally presented by Matt et al. 2001) are also in the sample of Nandra et al. (2007). In their analysis, only one observation shows evidence of broadened emission. Nandra et al. (2007) interpreted the lack of detection as simply the result of a low signal-to-noise ratio.

In this paper, we present the spectroscopic results of an *XMM–Newton* monitoring campaign of NGC 5506, which brings the total integration time to $\simeq$197 ks (versus the 23 ks of the observations published so far). The main result of this paper is the first unambiguous detection of a broad iron K_α line in NGC 5506.

2 OBSERVATIONS AND DATA REDUCTIONS

Table 1 lists the *XMM–Newton* observations of NGC 5506 performed so far. We discuss, in this paper, the data of the EPIC cameras only (MOS, Turner et al. 2001; pn, Strüder et al. 2001). Data were reduced using the SAS v9.0 (Gabriel et al. 2003) tasks E[MP]PROC with standard settings. Periods of high background were removed using count rate thresholds on the high-energy, single event, field-of-view light curves (Table 1), which optimize the signal-to-noise of each individual observation. Source spectra were extracted from circular regions surrounding the source centroid (Table 1), while background spectra were taken from circular regions on the same CCD chip, and are free from contaminating serendipitous sources (and at the same height in detector coordinates for the pn to ensure that the same charge transfer inefficiency correction applies). Response files were generated with the SAS tasks ARFGEN and RMFGEN. Spectra were rebinned to oversample the intrinsic energy resolution by a factor not larger than 3, and to ensure that each spectral channel has a number of background-subtracted counts larger than 50. Spectral fits were performed in the 2.2–10 keV energy band, to avoid large gradients of the instrument transfer function as a result of the instrumental edges (1.8–2.2 keV) and to the soft X-ray photoelectric cut-off. Below the energy of the latter, the X-ray spectrum is dominated by reprocessing and scattering of the nuclear radiation by photoionized gas on scales as large as a few hundred parsec (Bianchi et al. 2003). High-resolution spectroscopy of this component will be discussed elsewhere (Labiano et al., in preparation).

In this paper, energies are quoted in the source rest frame and errors are quoted at the 90 per cent confidence level for one interesting parameter. The following cosmological parameters have been adopted in the calculation of the luminosities: $H_0 = 70$ km s^{-1} Mpc^{-1}, $\Lambda_0 = 0.73$ and $\Omega_{\rm m} = 0.27$ (Bennett et al. 2003).

3 SPECTRAL ANALYSIS

3.1 Phenomenological fits on individual observations

As a first step, we fit the pn spectrum of each individual *XMM–Newton* observation with the same phenomenological model. Following the approach in Matt et al. (2001), the model is constituted by a photoelectrically absorbed power law, a photoelectric absorption edge and three narrow iron emission lines, modelling the K_α fluorescence of Fe I and of the recombination lines of Fe XXV and Fe XXVI. Fe I and Fe XXVI are actually each close doublets, which cannot be resolved by the EPIC cameras. Their centroid energy has been fixed to the weighed mean of the corresponding doublet components: 6.399 and 6.966 keV, respectively. The structure of the Fe XXV line is instead more complex, with the resonance (6.7002 keV), two intercombination (6.6821 and 6.6673 keV) and the forbidden components (6.6364 keV) all potentially contributing. In the fit of each observation, we originally left the Fe XXV centroid energy free to vary. We obtained lower limits consistent with the energy of the resonance line (and inconsistent with the other components) in all observations, except in XMM8, where $E_{\rm c}^{\rm Fe\,XXV} = 6.654 \pm ^{0.020}_{0.017}$ keV [$I = (3.7 \pm 1.0) \times 10^{-5}$ photons cm^{-2} s^{-1}]. In all the subsequent models, we fixed the centroid energy of the Fe XXV line to the value of the resonance component, except for XMM8, for which we used the value of the forbidden component. Finally, the energy of the edge was constrained to be $\gtrsim$7.11 keV, corresponding to the photoionization of iron.

The Fe I line 1σ width (only 'width' hereafter) is $46 \pm ^{11}_{14}$ eV. This measurement is consistent with the width of the manganese K_α and K_β pn calibration emission lines measured in observations close to the 2009 NGC 5506 observations: $\sigma_{\rm cal} = 42 \pm 8$ eV and $\sigma_{\rm cal} = 47 \pm 8$ eV in Obs 0410780601 (2008 August 9) and Obs 0412580401 (2009 January 4), respectively. The measurement is thus consistent with the instrumental resolution. We have consequently used this value for all the nominally unresolved astrophysical emission lines in the models discussed in this paper.

[1]See, however, Nandra et al. (2007), whose spectral deconvolution of the *XMM–Newton*/EPIC spectra requires $\imath \lesssim 20^\circ$.

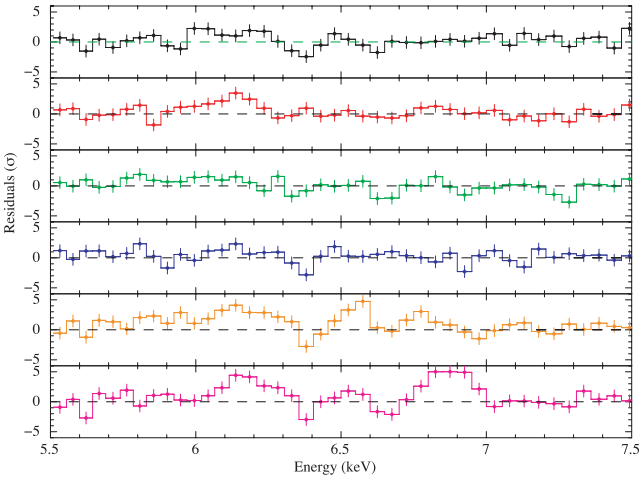

Figure 1. 5.5–7.5 keV residuals in units of standard deviation when the best-fitting phenomenological model is applied to the 2.2–12 keV EPIC–pn spectra of the 2004–2009 *XMM–Newton* observations of NGC 5506.

Fig. 1 shows the residuals against the best-fitting phenomenological model in the 5.5–7.5 keV energy band (the residuals are flat outside this interval). In the longest observations, significant wave-like residuals are present around the nominal energy of the Fe I fluorescent K_α line. Hints of features with a similar shape are visible in other observations with a lower statistics. These features can be interpreted as being the result of a broad ($\sigma \simeq 300$ eV) excess emission feature, which the narrow Fe I Gaussian profile is unable to account for.

Fig. 1 does not show the residuals for the first two observations (XMM1 and XMM2). The event pattern distribution measured by the SAS task EPATPLOT suggests that they might be marginally affected by pile up because of the different instrument mode (large window instead of small window). This may also explain why XMM2, which corresponds to the highest X-ray flux measured during our campaign, exhibits the flattest X-ray spectral index. This is illustrated in Fig. 2, which shows the best-fitting parameters of the phenomenological model in each individual fit as a function of time and of the 7–12 keV absorption-corrected flux, once the excess emission around 6 keV is fit with a further Gaussian profile whose width was left free to vary.

The intensity of the narrow Fe I line is constant. Its mean normalized dynamical range is $\leq$27 per cent. Evidence for variability of the recombination He- and H-like line intensity is also marginal. Beside the possible change of ionization state of Fe XXV in XMM8, it is limited to a nominal difference by a factor of at least 5 between two measurements of the Fe XXVI line during the 2004 monitoring campaign. Given the uncertainties in the spectral deconvolution at $\simeq$7 keV, we consider this evidence for variability as only tentative, to be confirmed by high-resolution measurements.

We have applied the same phenomenological model also to the combined spectra extracted from the MOS cameras. The parameters of the continuum are different. The ratio between the 2–10 keV MOS and pn fluxes (weighted mean, $\langle F_{\rm MOS}/F_{\rm pn}\rangle$ = 5.5 per cent; $\sigma_{F_{\rm MOS}/F_{\rm pn}} = 2.7$ per cent) is consistent with known systematic calibration uncertainties in the absolute flux determination (Stuhlinger et al. 2008). However, the average difference between the spectral index ($\langle\Delta\Gamma\rangle = 0.23$; $\sigma_{\Delta\Gamma} = 0.07$) and the column density ($\langle\Delta N_{\rm H}\rangle = 4.9\times10^{21}$ cm^{-2}; $\sigma_{\Delta N_{\rm H}} = 2.0\times10^{21}$ cm^{-2}) is larger than expected. The difference is larger for higher fluxes. The continuum spectral parameters measured by the EPIC cameras are instead very consistent for observations whose 2–10 keV flux is lower than $\simeq 8\times10^{-11}$ erg cm^{-2} s^{-1}. Visual inspection of the MOS pattern fraction distribution unveiled an excess (deficit) of double (single) events by 15–30 per cent above 4 keV in higher flux observations. The above pieces of evidence indicate that many of the NGC 5506 MOS spectra could be still affected by pile up. Consequently, we do not discuss the MOS spectra in the rest of the paper. However, we show in Section 3.2 that the main result of this

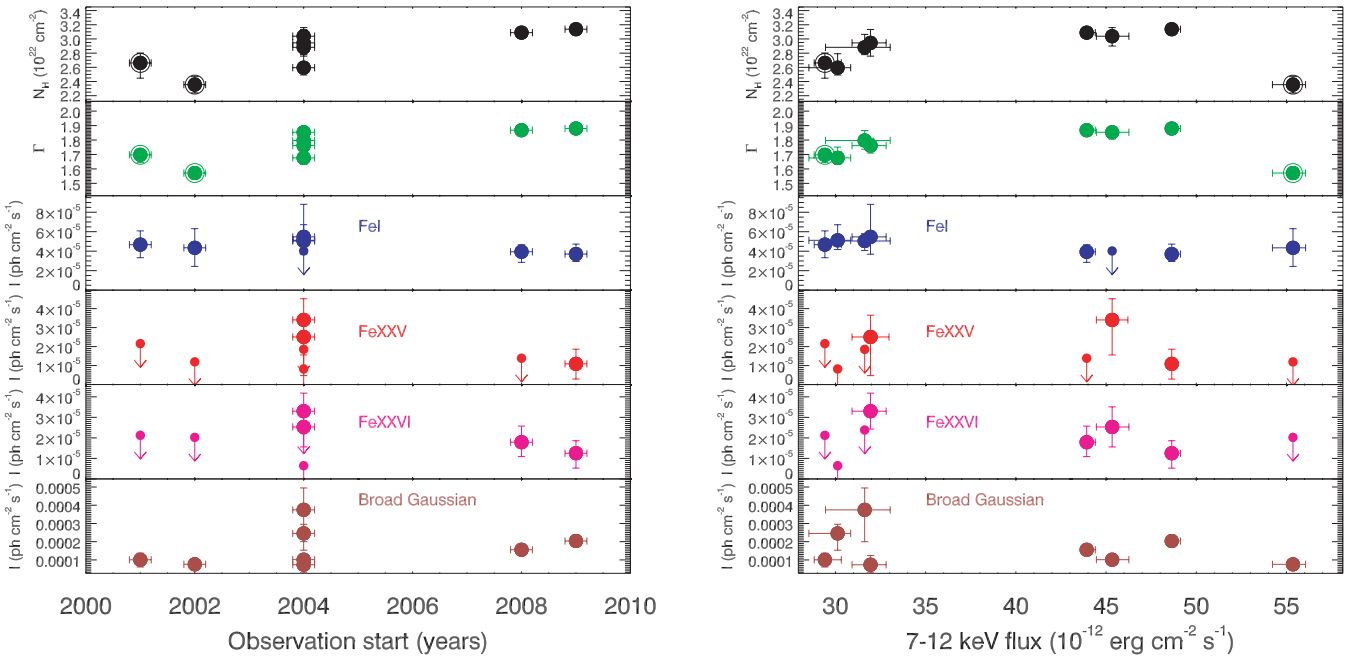

Figure 2. Best-fitting parameters of the phenomenological fits of individual NGC 5506 *XMM–Newton* observations as a function of time (left) and of the 7–12 keV absorption-corrected flux (right). From top to bottom: photon index, column density, intensity of the Fe I, Fe XXV, Fe XXVI narrow emission lines and of the broad Gaussian. Continuum measurement data points corresponding to pn observations in Large Window mode are surrounded by a large circle.

paper (the ultimate discovery of a broad component of the iron K_α line) is measured in both the pn and MOS cameras with comparable properties.

3.2 Physically motivated combined fits of all observation spectra

3.2.1 Description of the models

Motivated by the results presented in the previous section, we enriched the phenomenological model by adding physically motivated components to account for features detected in the spectral residuals. We have investigated three main scenarios, as follows.

(i) Scenario 1: relativistically broadened K_α iron line and non-relativistic Compton reflection. The former component has been modelled through the code KYRLINE (Dovčiak, Karas & Yaqoob 2004), which calculates the profile of an emission line produced in an axisymmetric accretion disc around a black hole. The Compton-reflection component (model PEXRAV; Magdziarz & Zdziarski 1995) is primarily associated in this scenario to the narrow core of the iron K_α line. However, it may include a contribution by the accretion disc as well, which the moderate energy resolution of the EPIC cameras is unable to disentangle.

(ii) Scenario 2: non-relativistically broadened K_α iron line and Compton reflection. The former component has been modelled with a simple Gaussian profile.

(iii) Scenario 3: relativistically broadened emission-line and continuum reflection dominated by a relativistically blurred component. The latter component has been modelled by convolving PEXRAV with the relativistic kernel KYCONV (Dovčiak et al. 2004) and assuming a constant ratio between the normalization of the primary continuum and that of the Compton reflection (R; see Table 2).

Table 2. Best-fitting results for the parameters of the non-relativistic continuum components in scenario 3 (except parameter $EW_{\rm Fe\,I}$, which refers to scenario 1).

Spectrum-dependent parameters			
Obs.	$N_{\rm H}$ (10^{22} cm^{-2})	Γ	2–10 keV flux[a] (10^{-12} erg s^{-1} cm^{-2})
XMM3	$2.86 \pm ^{0.11}_{0.14}$	$1.778 \pm ^{0.014}_{0.025}$	$82.5 \pm ^{0.6}_{1.2}$
XMM4	$2.94 \pm ^{0.12}_{0.14}$	$1.777 \pm ^{0.013}_{0.033}$	$79.4 \pm ^{1.2}_{1.1}$
XMM5	$2.65 \pm ^{0.12}_{0.14}$	$1.771 \pm ^{0.014}_{0.027}$	$71.4 \pm ^{0.7}_{1.3}$
XMM6	$2.99 \pm ^{0.08}_{0.12}$	$1.844 \pm ^{0.016}_{0.015}$	$120.0 \pm ^{0.6}_{1.3}$
XMM7	$3.08 \pm ^{0.04}_{0.03}$	1.864 ± 0.009	$132.5 \pm ^{1.3}_{0.9}$
XMM8	$3.04 \pm ^{0.06}_{0.05}$	$1.862 \pm ^{0.010}_{0.006}$	$118.7 \pm ^{0.3}_{0.7}$
Spectrum-independent parameters			
$I^b_{\rm Fe\,I} = (5.9 \pm 0.6) \times 10^{-5}$ erg cm^{-2} s^{-1}			
$I^b_{\rm Fe\,XXVr} \leq 1.0 \times 10^{-5}$ erg cm^{-2} s^{-1}			
$I^b_{\rm Fe\,XXVf} \leq 1.4 \times 10^{-5}$ erg cm^{-2} s^{-1}			
$I^b_{\rm Fe\,XXVI} = (2.0 \pm 0.7) \times 10^{-5}$ erg cm^{-2} s^{-1}			
$R \leq 0.1$[c]			
$EW_{\rm Fe\,I} \geq 1.0$ keV[d]			

[a] Corrected for absorption: XMM1, 70.8 ± 1.0; XMM2, $121.1 \pm ^{1.4}_{1.1}$ in the same units.
[b] Intensity of the narrow emission lines.
[c] Ratio between the primary continuum and the relativistically blurred reflection normalization.
[d] Equivalent width of the narrow component of the Fe I fluorescent line against its own reflection continuum.

KYRLINE belongs to a suite of models based on a common ray-tracing subroutine, aimed at describing the X-ray emission of black-hole accretion discs in the strong gravity regime (Dovčiak et al. 2004). The line profile depends on the following parameters: (i) the black hole spin a (comprised between 0 and 0.9982 in dimensionless relativistic units); (ii) the inner ($r_{\rm in}$) and outer ($r_{\rm out}$) radii of an annular region on the disc where the line photons are emitted; (iii) the index α of the radial dependence of the emissivity per unit area, κ, in the local frame comoving with the disc: $\kappa(r) \propto r^{-\alpha}$; (iv) the 'disc inclination' $\imath$ (i.e. the angle between the normal to the disc plane and the line of sight); (v) the rest-frame energy (assumed monochromatic) of the photons emitted by the disc, $E_{\rm c}$. Although the line normalization in KYRLINE is expressed in units of photons cm^{-2} s^{-1} integrated over the whole profile, we also use the line equivalent width (EW; i.e. the line intensity normalized to the underlying continuum at 6.4 keV) to make comparison with theoretical predictions easier (Matt et al. 1992). The convolution function KYCONV uses the same relativistic kernel as KYRLINE.

The continuum reflection components replace the photo-absorption edge in the phenomenological model. We have always linked together the spectral index of the Compton-reflected continuum and that of the primary emission. Moreover, we have added two narrow-band spectral components to the non-relativistic emission-line complex, modelling the following: (i) the iron K_α fluorescent iron line Compton-shoulder (Sunyaev & Churazov 1996; Matt 2002) through a rectangular box function comprised between 6.24 and 6.4 keV, whose intensity was constrained to be no larger than 20 per cent of the intensity of the corresponding narrow K_α line (the fits determine only an upper limit on this parameter as large as the maximum allowed value); (ii) the K_β line associated with the iron K_α narrow component, modelled with a Gaussian profile with energy fixed at 7.058 keV and intensity constrained not to exceed 16 per cent of the K_α intensity (Molendi, Bianchi & Matt 2003).

In principle, only the model parameters describing physical quantities not expected to change among the observations (or demonstrated to remain constant in the phenomenological analysis) have been constrained to have the same value for all fitted spectra. These are the intensities of the narrow Fe I, Fe XXV and Fe XXVI lines, the metallicity (assumed solar; Anders & Grevesse 1989), the high-energy cut-off of the intrinsic primary continuum (held fixed to 130 keV in accordance with the results of the *BeppoSAX* observation; Bianchi et al. 2003), the inclination of the disc and of the distant non-relativistic reflector (the latter held fixed to 45°) and the black hole spin. In scenarios 1 and 3, varying the black hole spin from Schwarzschild to maximally rotating yields a variation of χ^2 lower than 0.5. We have therefore fixed this parameter to the value corresponding to the latter solution ($a = 0.998$), favoured at face value. Once these assumptions were made, a first series of fits showed that many of the remaining free parameters were consistent with being constant across all the fitted observations. We have therefore forced these to assume the same value in all the fits. In scenarios 1 and 3, these are the following.

(i) The inner and outer radii of the X-ray emitting disc. Initially we have fixed the latter to $400r_g$, because this parameter is generally unconstrained when the line profile is strongly relativistic. We review this assumption in Section 3.2.2. The former has been constrained throughout the paper to coincide with the innermost stable circular orbit of an accretion disc corotating with a black hole of spin a.

(ii) The index of the power-law disc emissivity radial dependence, α.

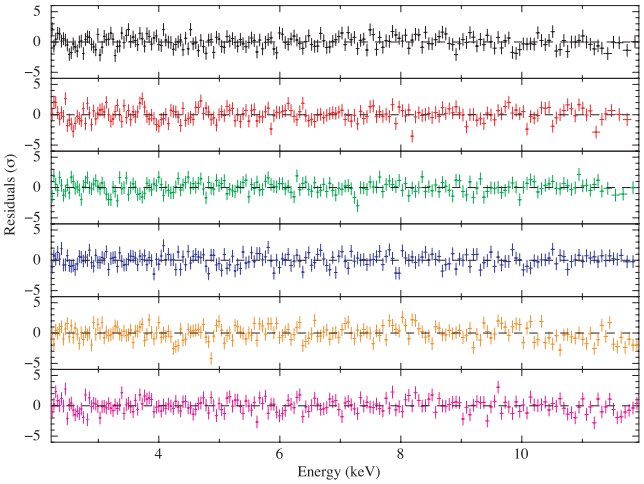

Figure 3. Residuals in units of standard deviation when the scenario 3 best-fitting model is applied to the 2004–2009 EPIC–pn spectra. From top to bottom: XMM3, XMM4, XMM5, XMM6, XMM7 and, XMM8. The *Y*-axis range and colours are the same as in Fig. 1.

(iii) The energy of the relativistically broadened line in the source rest frame, E_c.

In scenario 2, these are all the parameters describing the broad Gaussian profile.

3.2.2 *Results*

The scenarios described above yield comparable fit qualities: $\chi^2/\nu = 1265.3/1161$, 1280.9/1161 and 1258.1/1161 for scenarios 1, 2 and 3, respectively. These χ^2 are significantly better than those yielded by the same models without the broad line: 1479.5/1169, 1516.2/1169 and 1581.6/1166, respectively. No further structure is visible in the residuals (Fig. 3). Therefore, we have concluded that no additional astrophysical component is required. In Table 2 we summarize the best-fitting results for the non-relativistic components in scenario 3. The values for the other scenarios are consistent with these, within the statistical uncertainties. Fig. 4 shows the spectra of observations XMM3–XMM8, together with the components of their best-fitting models.

The properties of the relativistic line can be summarized as follows (see Table 3). (i) The rest-frame centroid energy is consistent with neutral or moderately ionized iron ($E_c \simeq 6.48$ keV). Fixing the source frame centroid energy to the value expected for neutral iron in, for example, scenario 3 yields $\chi^2 = 1276.0/1160$ dof. (ii) The disc is slightly more inclined ($\iota \simeq 40^\circ$) than typically measured in unobscured Seyfert galaxies (Nandra et al. 1997, 2007). (iii) The line profile is only mildly relativistic as parametrized by the moderately flat ($\alpha \simeq 1.9$) radial emissivity profile. The line emitting region extends close to the innermost stable orbit. The innermost radius is constrained between 3 and $25r_g$. Fig. 5 shows the profile of the relativistically broadened iron line, obtained by stacking together the source frame residuals of each individual observation against the best-fitting model in scenario 3, once the relativistically broadened emission line is removed from the model. The profile is not significantly skewed. This is consistent with the similar fit quality that relativistic and non-relativistic scenarios yield. A small 'dip' in the profile coincides exactly with the rest-frame energy of the K_α neutral iron fluorescent line. This could be the result of an incorrect disentangling between the narrow and broad profiles, whereby the fit preferentially attributes photons in this energy range to the former. We estimate that the intensity of the narrow component should be lowered by at least 50 per cent for the dip to disappear. The effect of this potential systematic uncertainty on the determination of the relativistic line profiles α and r_{in} is negligible, because they are mostly sensitive to the red wing. However, the centroid energy and inclination angle could be affected. Assuming $I_{Fe\,I} = 3 \times 10^{-5}$ photons cm^{-2} s^{-1}, these change by $\Delta E_c \simeq 30$ eV and $\Delta\iota \simeq 4^\circ$, respectively. None the less, χ^2 significantly worsens (1361.9/1160 dof in scenario 3). This hypothesis is then inconsistent with the data.

We return now to the original restriction imposed on the value of r_{out}. The flat value of α implies that a non-negligible contribution to the broad line profile comes also from large disc radii. We have therefore repeated the fits in scenario 3, after allowing r_{out} to be a free parameter. At the 90 per cent confidence level for one interesting parameter r_{out} is constrained to be comprised between 250 and $900r_g$. The best-fitting value is still around $400r_g$, and hence the best-fitting values do not change. However, the broad-line parameter errors are augmented by a small amount (Table 3).

In scenario 2, the centroid energy of the Gaussian profile is consistent with fluorescence from neutral or moderately ionized iron: $E_c = 6.45 \pm ^{0.04}_{0.05}$ keV. The linewidth is $\sigma_b = 330 \pm 40$ eV.

We have checked the robustness of the broad iron line profile against possible data reduction and/or undiagnosed calibration problems. A fit with scenario 2 on a merged pn spectrum with single and double events yields the following best-fitting broad Gaussian profile parameters: $E_c = 6.47 \pm ^{0.04}_{0.03}$ keV, $\sigma_b = 360 \pm ^{40}_{30}$ eV and $I_b = (1.47 \pm 0.14) \times 10^{-4}$ ph s^{-1} cm^{-2}. These agree within the statistical uncertainties with the best-fitting parameters obtained on a merged pn spectrum extracted with single events only: $E_c = 6.41 \pm 0.04$ keV, $\sigma_b = 360 \pm ^{50}_{70}$ eV and $I_b = (1.55 \pm 0.18) \times 10^{-4}$ ph s^{-1} cm^{-2}. More importantly, the width measured by the pn spectrum agrees with that simultaneously measured by the MOS cameras (Fig. 6).

3.2.3 *Variability*

The EW of the broad component of the iron K_α line is consistent with being constant among the *XMM–Newton* observations discussed in this paper (Table 4). However, its intensity is not constant. A fit on the broad line intensity versus time relation with a constant yields $\chi^2/\nu = 11.4/5$ (versus 2.1/5 for the EW). This indicates that, in the first approximation, the broad line intensity follows the variation of the underlying continuum.

The absorption-corrected 2–10 keV flux measured during the *XMM–Newton* observations covers a dynamical range $\simeq$1.9. This is less than a factor of 2 smaller than that measured during the 6-yr long intense X-ray monitoring using the Proportional Counter Array (PCA) of the *Rossi X-ray Timing Explorer* (*RXTE*) in the same energy band ($\simeq$3.5; Uttley & McHardy 2005). The longest time difference between two observations, whose continuum flux differs by more than 27 per cent (the upper limit on the percentage fractional variability of the intensity of the iron K_α fluorescent line narrow component) is $\simeq$7.92 yr (XMM8 versus XMM1).

The photon index in observations XMM6–XMM8 (2–10 keV absorption-corrected flux, $F_{2-10} \geq 1.19 \times 10^{-10}$ erg s^{-1} cm^{-2}) is systematically steeper than in the others (by $\Delta\Gamma \simeq 0.08$–0.10). There is an intrinsic correlation between the power-law spectral index and the column density of a photoelectric absorber covering it as measured by the spectral fitting. Steep spectra invariably correspond to higher obscuration. In order to disentangle the intrinsic driver of the continuum spectral variability, we run two scenario

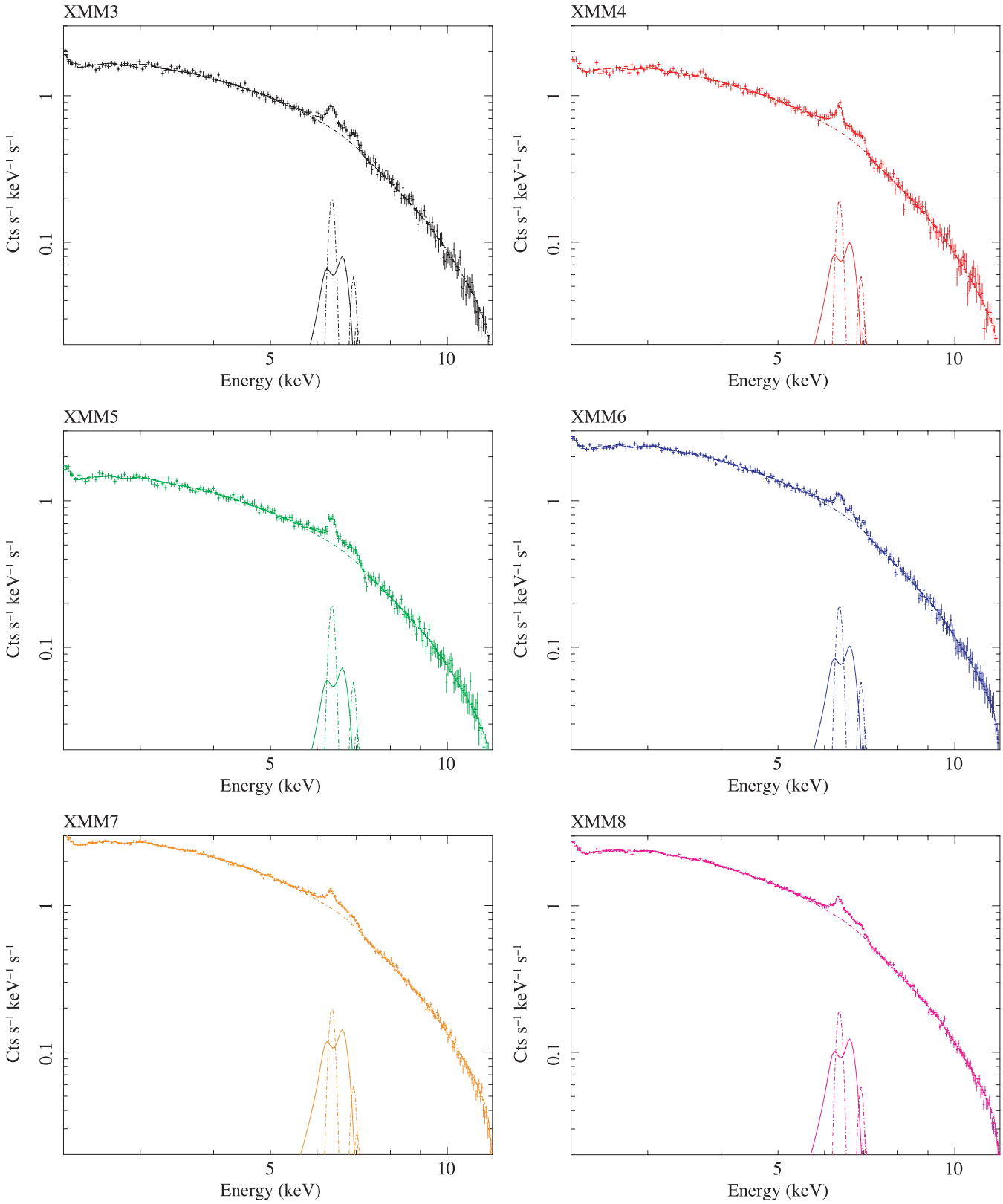

Figure 4. EPIC–pn NGC 5506 spectra in observations XMM3–XMM8 (crosses). The lines indicate different model components: dot-dashed, continuum; long dot-dashed, narrow lines; solid, broad line.

Table 3. Best-fitting values of the K_α iron relativistically broadened profile in scenarios 1 and 3 for $r_{out} = 400 r_g$. The rightmost column contains the statistical uncertainties to be added if r_{out} is allowed to vary.

	Scenario 1	Scenario 3	Additional error if r_{out} is left free
E_c (keV)	6.48 ± 0.02	6.48 ± 0.02	$\pm^{0.02}_{0.00}$
α	1.9 ± 0.3	1.9 ± 0.3	$\pm^{0.2}_{0.1}$
ι °	$42 \pm ^{2}_{6}$	$37 \pm ^{6}_{5}$	$\pm^{11}_{4}$
r_{in} (r_g)	$15 \pm ^{9}_{12}$	$15 \pm ^{11}_{9}$	$\pm^{7}_{1}$

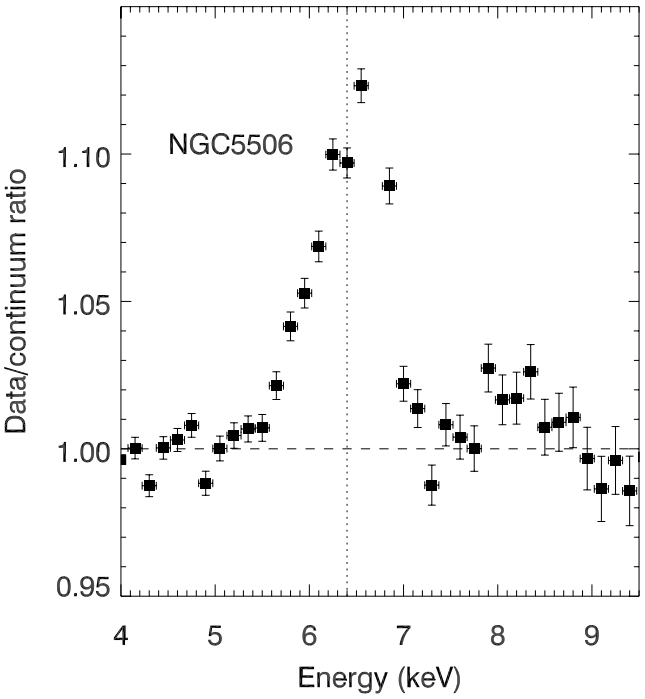

Figure 5. Stacked profile of the relativistically broadened iron line. The dashed line indicates the observed frame energy of the neutral iron K_α fluorescent line.

3 models, where the power-law index or the column density have been constrained to assume alternatively the same value among all spectra. The quality of the fit (albeit worse than when both parameters are allowed to vary) is better in the case when the power law is allowed to vary: $\chi^2/\nu = 1276.4$ against 1300.6/1164. This suggests that variations of the intrinsic continuum are the main driver of this long-term continuum spectral variability.

The X-ray light curve of NGC 5506 also shows rapid variability, by a factor of $\simeq$1.7 over 250 s ($\Delta L_X \simeq 1.1 \times 10^{42}$ erg s^{-1}; Dewangan & Griffiths 2005). The variability is achromatic (Fig. 7; McHardy & Czerny 1987). In order to investigate the possible dependence of the broad line parameters upon the overall source flux on such small time-scales, we have combined the event lists of the 2009 observations, and extracted four intensity-resolved spectra, corresponding to the following background-subtracted count rate ranges: <2.9, 2.9–3.2, 3.2–3.5 and >3.5 s^{-1}. These ranges were chosen in such a way that the intensity-resolved spectra have approximately the same net background-subtracted counts. These spectra are labelled as XMM78$_j$ in Table 4, with $j = 1$–4 (in increasing flux order). The corresponding 2–10 keV absorption-corrected fluxes are $109.3 \pm ^{1.3}_{1.4}$, $124.3 \pm ^{1.3}_{1.6}$, $134.6 \pm ^{1.6}_{1.8}$ and $145.0 \pm ^{1.3}_{1.7} \times 10^{-12}$ erg cm^{-2} s^{-1},

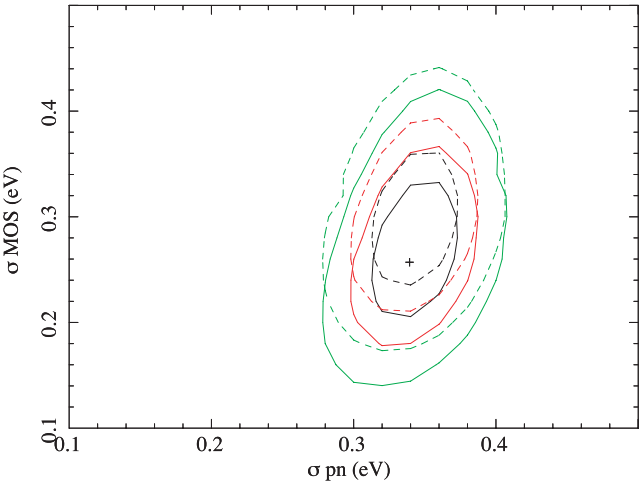

Figure 6. Iso-χ^2 contour plots for the intrinsic width of a Gaussian profile fitting the broad component of the iron K_α line in the NGC 5506 merged spectra. The contours correspond to the 68, 90 and 99 per cent confidence levels for two interesting parameters, respectively. Solid lines, pn versus MOS1; dashed lines, pn versus MOS2.

Table 4. Measurements of the broad iron K_α line EW (in eV).

Obs.	Scenario 1	Scenario 2	Scenario 3
XMM3	$130 \pm ^{40}_{20}$	130 ± 30	$120 \pm ^{30}_{20}$
XMM4	$180 \pm ^{30}_{40}$	160 ± 30	$150 \pm ^{30}_{20}$
XMM5	140 ± 30	130 ± 30	120 ± 30
XMM6	$122 \pm ^{17}_{26}$	$100 \pm ^{30}_{20}$	110 ± 20
XMM7	$152 \pm ^{11}_{12}$	$137 \pm ^{13}_{15}$	$132 \pm ^{13}_{17}$
XMM8	$149 \pm ^{18}_{15}$	$143 \pm ^{12}_{16}$	131 ± 15
XMM78$_1$	$180 \pm ^{20}_{30}$	$140 \pm ^{30}_{20}$	160 ± 20
XMM78$_2$	$117 \pm ^{13}_{26}$	$90 \pm ^{30}_{20}$	$100 \pm ^{30}_{20}$
XMM78$_3$	$110 \pm ^{30}_{20}$	90 ± 20	$101 \pm ^{18}_{20}$
XMM78$_4$	120 ± 20	100 ± 20	$109 \pm ^{16}_{19}$

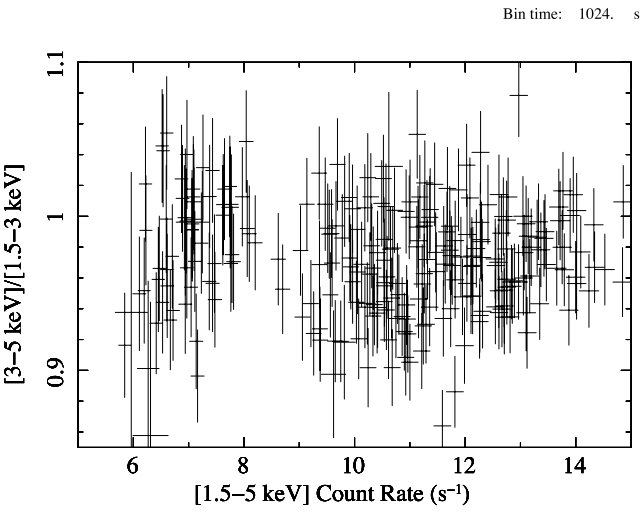

Figure 7. 3–5 keV versus 1.5–3 keV hardness ratio as a function of the 1.5–5 keV count rate in all the *XMM–Newton* observations of Table 1.

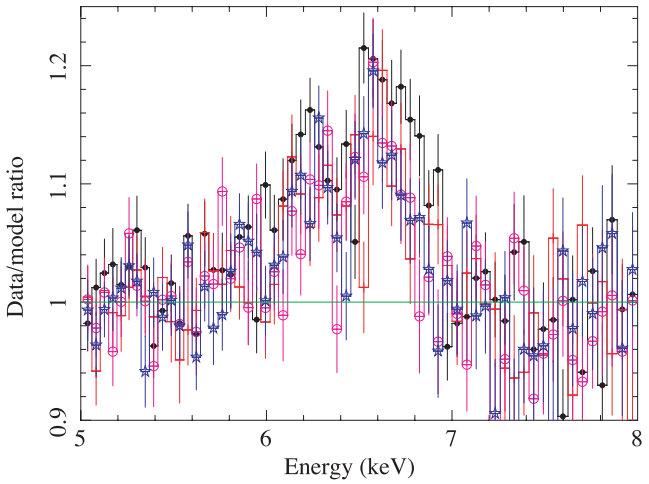

Figure 8. Residuals (in units of data/model ratio) when the best-fitting continuum in scenario 3 is applied to intensity-resolved spectra in the nominal energy range excised of the 5–7 keV interval. The contribution of the non-relativistic emission-line components was removed as well by subtracting their time-averaged intensity from the residuals. Filled circles, $XMM78_1$; crosses, $XMM78_2$; empty circles, $XMM78_3$; stars, $XMM78_4$.

respectively. No correlation exists between the EW of the broad K_α iron line component and the flux (Table 4), save for a larger EW in the spectrum corresponding to the lowest flux state. The shape of the broad line component remains also remarkably constant in different flux states (Fig. 8).

4 DISCUSSION

4.1 Continuum variability

NGC 5506 is one of the most rapidly variable AGNs of the X-ray sky. It exhibits luminosity changes of $\sim 10^{42}$ erg s^{-1} within a few minutes (Dewangan & Griffiths 2005). The variability is, however, remarkably achromatic on these time-scales (Fig. 7; see also McHardy & Czerny 1987). On longer time-scales, a small but systematic difference in the intrinsic spectral shape ($\Delta\Gamma \simeq 0.1$) is found between 'low-flux' and 'high-flux' observations (absorption-corrected flux ratio between these of about 1.5). An even larger dynamical range in both luminosity and spectral shape was measured during a hard X-ray ($E > 20$ keV) monitoring campaign with the high-energy X-ray imaging telescope (HEXIT; Manchanda 2006). The variability pattern measured by *XMM–Newton* is inconsistent with a pair-dominated corona (Haardt, Maraschi & Ghisellini 1997), where an increase of the spectral index by the amount observed by *XMM–Newton* requires at least an order-of-magnitude increase of the 2–10 keV luminosity. This does not automatically imply that pairs are not an important source of scattering in the Comptonizing material; the alternative possibility is that the increase of the corona optical depth is the result of a variation of the linear dimension of the corona. However, the shape of the broad iron K_α iron line does not change significantly on the shortest possible variability time-scales that *XMM–Newton* can probe (Fig. 8), suggesting that the illumination of the disc does not significantly change.

4.2 Origin of the narrow iron K_α line

One of the main results presented in this paper is that the intensity of the narrow component of K_α in NGC 5506 remains constant during the whole 8 yr covered by the *XMM–Newton* campaign. This extends by a factor of 3 the longest baseline published so far – a $\sim$1000 d *RXTE* monitoring campaign at the end of the last century (Lamer, Uttley & McHardy 2000). The *RXTE*/PCA spectroscopic measurements were unable to disentangle the two components (narrow and broad) of the iron K_α line. None the less, Lamer et al. (2000) claimed that the strength of the continuum reflection component and the total EW of the iron lines were stronger during phases of low flux. The origin of the iron K_α emission line has challenged the ingenuity of observational and theoretical astronomers since its early discovery (Mushotzky 1982; Turner & Pounds 1989). Evidence that this spectral feature is almost invariably accompanied by a Compton reflection continuum component (Pounds et al. 1990; Nandra & Pounds 1994) in unobscured AGNs suggested an origin in optically thick material out of the line of sight. The origin of very broad and skewed profiles in the innermost region of the accretion disc is a matter of heated debate, which we have briefly summarized in Section 1 (we further discuss this point in Section 4.3). As far as narrower (typical FWHM $\lesssim$3000 km s^{-1}) and symmetric lines are concerned, possible physical locations for the line-emitting matter are the external regions of the accretion disc (Fabian et al. 1989), the broad line regions (BLRs) (Yaqoob et al. 2001; Bianchi et al. 2008) or the molecular torus (Ghisellini, Haardt & Matt 1994; Krolik, Madau & Życki 1994). These systems have sizes from a fraction to several tens of parsec. The lack of correlation between the FWHM of the iron K_α and that of the H_β lines (or the black hole mass) disfavours a general origin in the BLRs (Nandra 2006).

We can use the lack of variability of the narrow component of the iron K_α fluorescent line to estimate the dimension of its production region. The line produced by a reflector at distance d from an illuminating source tracks the variability pattern of the primary continuum if $d \lesssim t_{\rm var}/c$, where $t_{\rm var}$ is the continuum variability time-scale and c is the speed of light. We estimate $t_{\rm var}$ as the longest time interval between *XMM–Newton* observations, whose 2–10 keV absorption-corrected fluxes differ by more than 27 per cent (i.e. than the upper limit on the percentage fractional variability of the iron line intensity). $t_{\rm var}$ hence corresponds to the span between observations XMM1 and XMM8: 7.92 yr. This estimate is qualitatively in agreement with the determination of the power spectrum density by the *RXTE*/PCA monitoring campaign (Uttley & McHardy 2005), which exhibits a slope of $\simeq -1$ below $\nu \simeq 4 \times 10^{-5}$ Hz and down to $\simeq 6 \times 10^{-9}$ Hz. The *XMM–Newton* results constrain the location of the optically thick matter responsible for the bulk of the iron K_α narrow component at a distance $\gtrsim$2.5 pc. This is consistent with the best estimate of the inner side of the torus (<5 pc; Prieto & Meisenheimer 2004). Unfortunately, no direct estimate of the BLR size is available for NGC 5506. The 2–10 keV X-ray luminosity from the data presented in this paper is in the range $\simeq$6–11 $\times 10^{42}$ erg s^{-1}, which corresponds to a typical size of the BLR $\lesssim$ 10 d (Kaspi et al. 2005). This makes the torus the most likely origin of the narrow iron K_α line.

We report on a possible change in the intensity of the Fe XXVI during two of the observations in 2004 performed a few weeks apart, as well as a possible ionization change of the Fe XXV (from a resonance- to a forbidden-dominated state) during XMM8. Given, however, the spectral complexity around 7 keV, confirmation of these findings through instrumentation with a much better energy resolution is needed. This is shown, for instance, by the different results on the forbidden component of the He-like transition during XMM8 when we compare the phenomenological (Section 3.2) and relativistic (Table 2) models.

4.3 Origin of the broad iron Kα line

In this paper we report on the discovery of a broad ($\sigma \simeq 330$ eV) component of the iron K_α fluorescent emission line in NGC 5506. The line profile lacks a prominent red wing, in contrast to what is typically observed in unobscured Seyfert galaxies (Miller 2007). Although fits with a relativistically broadened profile yield marginally better statistical quality than symmetric Gaussian broadening, it is worth posing the question whether this difference may be the result of a different physical mechanism responsible for the observed broadening.

The symmetric and highly localized profile rules out an explanation in terms of blending of transitions corresponding to different iron ionization states, enhanced continuum reflection (Guainazzi 2002; Risaliti 2002), scattering from a relativistic wind (Titarchuk, Laurent & Shaposhnikov 2009) or incorrect fitting of the opacity affecting the underlying continuum (Turner & Miller 2009). Comptonization of line photons was suggested to explain the first observations of broad lines by *Ginga* (Czerny, Zbyszewska & Raine 1991). The observed moderate width requires the line photons to cross at most 3 Compton depths of cool ($kT_{\rm C} \leq 0.7$ keV; $\sigma = \sqrt{2}kT/mc^2$) gas (Pozdnyakov, Sobol & Sunyaev 1979; Sunyaev & Titarchuk 1980). The main shortcoming of this scenario, however, is the non-linear dependence of the line EW on the continuum flux on time-scales as short as a few hundreds of seconds, which is at odds with the line-emitting region being screened by optically thick matter.

The explanation in terms of a relativistically broadened and skewed profile is consistent with the data. Formal fits require a moderate inclination ($\imath \simeq 40^\circ$) accretion disc. NGC 5506 joins the so far restricted club of obscured AGNs, which require relativistic effects from a moderately inclined ($\imath \simeq 40^\circ$) accretion disc, together with MCG-5-23-16 (Balestra, Bianchi & Matt 2004) and NGC 526A (Nandra et al. 2007). All the above sources exhibit a column density obscuring the active nucleus in the range 10^{22-23} cm^{-2}. Although it is tempting to associate these sources with AGNs seen through the rim of the obscuring torus (see, for instance, the discussion in Matt, Guainazzi & Maiolino 2003), it should be borne in mind that several unobscured AGNs in Nandra et al. (2007) also formally require large inclination angles (e.g. Akn 120, Mkn 590, NGC 7213 and 7469). However, the recently discovered broad iron lines in IRAS 13197–1627 (Dadina & Cappi 2004; Miniutti et al. 2007a) and NGC 1365 (Risaliti et al. 2009) require moderate disc inclinations of $\imath \simeq 27^\circ$ and 24°, respectively. A comparison between unbiased samples is needed before any inference on the geometrical configuration of the torus and the disc in X-ray obscured AGNs can be drawn from X-ray spectroscopy of the relativistically broadened K_α line. Moreover, the disc inclination in NGC 5506 is significantly smaller than the inclination of the galaxy disc (Imanishi 2000).

The broad line is not extremely relativistic. It lacks the prominent red wing extending down to $\simeq$4 keV observed in, for example, MCG-6-30-15 (Fabian & Vaughan 2003; Miniutti et al. 2007a), which requires very steep radial emissivity profiles (Wilms et al. 2001). The inner radius of the line-emitting region (constrained by the data to be comprised between 3 and $25r_g$) and the flat emissivity profile suggest that a large area on the disc contributes to the average profile. The line profile is remarkably constant in intensity-resolved spectra, which sample variations of the intrinsic flux on time-scales as low as a few hundred seconds (cf. Fig. 8) (again at variance with MCG-6-30-15; Iwasawa et al. 1999). The fits do not require statistically significant changes in the structure of the innermost accretion flow. The parameters α and $r_{\rm in}$ describing the profile of the relativistically broadened iron line are consistent with being constant over five epochs of observations spanning 9 yr.

Little is known of the black hole mass in NGC 5506. Both the central stellar velocity dispersion ($\simeq$180 km s^{-1}; Oliva et al. 1999; Gebhardt et al. 2000; Ferrarese & Merrit 2000; Papadakis 2004) and the width of the [O III] line (Boroson 2003) suggest a black hole mass $\sim 10^8$ M$_\odot$. For this mass, the shortest measured X-ray variability time-scale implies that the bulk of high-energy continuum production and reprocessing occur within a few Schwarzschild radii from the black hole. This does not agree with the lack of extreme relativistic line broadening, as well as more generally with the idea that NLSy1 galaxies are characterized by small black hole masses and high accretion rates ($\lesssim$2 per cent in this scenario; Komossa 2007). However, X-ray-based estimates suggest that the black hole mass in NGC 5506 could be significantly lower. McHardy et al. (2006) observe that lowering the black hole mass by a factor of $\sim$5 would bring NGC 5506 to the locus in the PDS break frequency, black hole mass and accretion rate plane shared by AGNs and Galactic black hole systems. An even more radical revision ($M_{\rm BH} \simeq 5 \times 10^6$ M$_\odot$) has been proposed by Nikołajuk, Czerny & Gurynowicz (2009) on the basis of the correlation with the X-ray 2–10 keV light curve excess variance. A black hole mass of this order ($\sim 2 \times 10^6$ M$_\odot$) has been proposed by Hayashida et al. (1998) using similar arguments. The light crossing time of the shortest variability time-scale, if we assume the Nikołajuk et al. (2009) estimate, corresponds to about 20 Schwarzschild radii, in better agreement with broad iron line spectroscopy results. In this case, the accretion rate is $\simeq$40 per cent of the Eddington limit, if we estimate the bolometric luminosity by applying a luminosity-dependent bolometric correction to the 2–10 keV luminosity (Marconi et al. 2004). The size of the BLR, $r_{\rm BLR} \sim GM/v^2$, is $\sim$8 d, if we estimate v from the FWHM of the Paβ broad component (Nagar et al. 2002).

The size of the AGN sample with robust detections of relativistic lines is still far too small for correlations with other observables to yield stringent constraints. However, it is suggested that many of the objects of the Nandra et al. (2007) 'dream team' of relativistic AGNs are NLSy1s (Mkn 766, NGC 4051, 5506 and 7314) or at least characterized by extreme variability on short (MCG-6-30-15, NGC 4395) or long (NGC 2992) time-scales. Possible observational biases are discussed (and ruled out) by Nandra et al. (2007). A trend towards relativistically broadened lines being more common in narrow-line AGNs seems to be present in the stacked spectra of large samples of unobscured AGNs (Longinotti et al. 2008). However, there does not seem to be a correlation between the detection of relativistically broadened iron lines and either the accretion rate or the black hole mass in, for example, the Finding Extreme Relativistic Objects (FERO) sample (Longinotti et al. 2008). Once again, the small size and incompleteness of the available samples hamper firm conclusions.

ACKNOWLEDGMENTS

This work is based on observations obtained with *XMM–Newton*, a European Space Agency (ESA) science mission, with instruments and contributions directly funded by ESA member states and the National Aeronautics and Space Administration (NASA). Useful discussions with Michal Dovčiak and Giovanni Miniutti are gratefully acknowledged. A careful reading of the manuscript by an anonymous referee significantly improved the presentation of the results.

REFERENCES

Anders E., Grevesse N., 1989, Geochim. Cosmochim. Acta, 53, 197
Antonucci R., 1993, ARA&A, 31, 473
Antonucci R. R. J., Miller J. S., 1985, ApJ, 297, 621
Balestra I., Bianchi S., Matt G., 2004, A&A, 415, 437
Bennett C. L. et al., 2003, ApJS, 148, 1
Bianchi S., Balestra I., Matt G., Guainazzi M., Perola G. C., 2003, A&A, 402, 141
Bianchi S., La Franca F., Matt G., Guainazzi M., Jimenez Bailón E., Longinotti A. L., Nicastro F., Pentericci L., 2008, MNRAS, 389, L52
Boroson T. A., 2003, ApJ, 585, 647
Czerny B., Zbyszewska M., Raine D. J., 1991, in Treves A., ed., Iron Line Diagnostics in X-ray Sources. Springer-Verlag, Berlin, p. 226
Dadina M., Cappi M., 2004, A&A, 413, 921
Dewangan G. C., Griffiths R. E., 2005, ApJ, 625, L31
Dovčiak M., Karas V., Yaqoob T., 2004, ApJS, 153, 205
Fabian A. C., Vaughan S., 2003, MNRAS, 340, L28
Fabian A. C., Rees M. J., Stella L., White N. E., 1989, MNRAS, 238, 729
Ferrarese L., Merrit D., 2000, ApJ, 539, L9
Gabriel C., Denby M., Fyfe D. J., Hoar J., Ibarra A., 2003, inOchsenbein F., Allen M., Egret D., eds, ASP Conf. Ser. Vol. 314, Astronomical Data Analysis Software and Systems XIII. Astron. Soc. Pac., San Francisco, p. 759
Gebhardt K. et al., 2000, ApJ, 539, L13
Ghisellini G., Haardt F., Matt G., 1994, MNRAS 267, 743
Guainazzi M., 2002, MNRAS, 329, L13
Haardt F., Maraschi L., Ghisellini G., 1997, ApJ, 476, 620
Hayashida K., Miyamoto S., Kitamoto S., Negoro H., Inoue H., 1998, ApJ, 500, 642
Imanishi M., 2000, MNRAS, 313, 1651
Iwasawa K., Fabian A. C., Young A. J., Inoue H., Matsumoto C., 1999, MNRAS, 306, L19
Kaspi S., Maoz D., Netzer H., Peterson B. M., Vestergaard M., Jannuzi B. T., 2005, ApJ, 629, 61
Komossa S., 2007, RevMexAA Ser. Conf., 32, 86
Krolik J. H., Madau P., Życki P. T., 1994, ApJ, 420, L57
Lamer G., Uttley P., McHardy I. M., 2000, MNRAS, 319, 949
Longinotti A. L., de la Calle I., Bianchi S., Guainazzi M., Dočiak M., 2008, RevMexAA Ser. Conf., 32, 62
McHardy I., Czerny B., 1987, Nat, 325, 696
McHardy I., Koerding E., Knigge C., Uttley P., Fender R. P., 2006, Nat, 444, 730
Magdziarz P., Zdziarski A. A., 1995, MNRAS, 273, 837
Manchanda R. K., 2006, Adv. Space Res., 38, 1387
Marconi A., Risaliti G., Gilli R., Hunt L. K., Maiolino R., Salvati M., 2004, MNRAS, 351, 169
Matt G., 2002, MNRAS, 337, 147
Matt G., Perola G. C., Piro L., Stella L., 1992, A&A, 257, 63 (erratum, A&A, 263, 453)
Matt G., Guainazzi M., Perola G. C., Fiore F., Nicastro F., Cappi M., Piro L., 2001, A&A, 377, L31
Matt G., Guainazzi M., Maiolino R., 2003, MNRAS, 342, 422
Miller J. M., 2007, ARA&A, 45, 441
Miniutti G. et al., 2007a, PASJ, 59, 315
Miniutti G., Ponti G., Dadina M., Cappi M., Malaguti G., 2007b, MNRAS, 375, 227
Molendi S., Bianchi S., Matt G., 2003, MNRAS, 343, L1
Mushotzky R. F., 1982, ApJ, 256, 92
Mushotzky R. F., Fabian A. C., Iwasawa K., Kunieda H., Matsuoka M., Nandra K., Tanaka Y., 1995, MNRAS, 272, L9
Nagar N. M., Oliva E., Marconi A., Maiolino R., 2002, A&A, 391, L21
Nandra K., 2006, MNRAS, 368, L62
Nandra K., Pounds K. A., 1994, MNRAS, 268, 405
Nandra K., George I. M., Mushotzky R. F., Turner T. J., Yaqoob T., 1997, ApJ, 467, 70
Nandra K., O'Neill P. M., George I. M., Reeves J. N., 2007, MNRAS, 382, 194
Nikołajuk M., Czerny B., Gurynowicz P., 2009, MNRAS, 394, 2141
Oliva E., Origlia L., Maiolino R., Moorwood A. F. M., 1999, A&A, 350, 9
Papadakis I. E., 2004, A&A, 425, 1133
Pounds K. A., Nandra K., Stewart G. C., George I. M., Fabian A. C., 1990, Nat, 344, 132
Pozdnyakov L. A., Sobol I. M., Sunyaev R. A., 1979, A&A, 75, 214
Prieto M. A., Meisenheimer K., 2004, IAUS, 222, 57
Reeves J. N., Nandra K., George I. M., Pounds K., Turner T. J.,Yaqoob T., 2004, ApJ, 602, 648
Reeves J. N. et al., 2007, PASJ, 59, 301
Reynolds C. S., Nowak M. A., 2003, Phys. Rep., 377, 389
Risaliti G., 2002, A&A, 386, 379
Risaliti G. et al., 2009, ApJ, 696, 160
Strüder L. et al., 2001, A&A, 365, L18
Stuhlinger M. et al., 2008, Status of *XMM–Newton* instrument cross-calibration. ESAC-ESA, Villafranca del Castillo (available at http://xmm2.esac.esa.int/docs/documents/CAL-TN-0052.ps.gz)
Sunyaev R. A., Churazov E. M., 1996, Astron. Lett., 22, 649
Sunyaev R. A., Titarchuk L. G., 1980, A&A, 86, 121
Tanaka Y. et al., 1995, Nat, 375, 659
Titarchuk L., Laurent P., Shaposhnikov N., 2009, ApJ, 700, 1831
Turner T. J., Miller L., 2009, A&AR, 17, 47
Turner T. J., Pounds K., 1989, MNRAS, 240, 833
Turner M. J. L. et al., 2001, A&A, 365, L27
Uttley P., McHardy I. M., 2005, MNRAS, 363, 586
Wang T., Mihara T., Otani C., Matsuoka M., Awaki H., 1999, ApJ, 515, 567
Wilms J., Reynolds C. S., Begelman M. C., Reeves J., Molendi S., Staubert R., Kendziorra E., 2001, MNRAS, 328, L27
Yaqoob T., George I. M., Nandra K., Turner T. J., Serlemitsos P. J., Mushotzky R. F., 2001, ApJ, 546, 759

This paper has been typeset from a TEX/LATEX file prepared by the author.